HIV-1 Nef Promotes Endocytosis of Cell Surface MHC Class II Molecules via a Constitutive Pathway

Ashutosh Chaudhry, Divya Anna Verghese, Suman Ranjan Das, Shahid Jameel, Anna George, Vineeta Bal, Satyajit Mayor and Satyajit Rath

References	This article **cites 44 articles**, 21 of which can be accessed free at: http://www.jimmunol.org/content/183/4/2415.full.html#ref-list-1
	Article cited in: **http://www.jimmunol.org/content/183/4/2415.full.html#related-urls**
Correction	A correction has been published for this article. The contents of the correction have been appended to the original article in this reprint. The correction is also available online at: **http://www.jimmunol.org/content/183/11/7611.1.full.html**
Subscriptions	Information about subscribing to *The Journal of Immunology* is online at http://www.jimmunol.org/subscriptions
Permissions	Submit copyright permission requests at http://www.aai.org/ji/copyright.html
Email Alerts	Receive free email-alerts when new articles cite this article. Sign up at http://www.jimmunol.org/etoc/subscriptions.shtml/

HIV-1 Nef Promotes Endocytosis of Cell Surface MHC Class II Molecules via a Constitutive Pathway[1]

Ashutosh Chaudhry,[2]* Divya Anna Verghese,[2]* Suman Ranjan Das,[†] Shahid Jameel,[†] Anna George,* Vineeta Bal,* Satyajit Mayor,[‡] and Satyajit Rath[3]*

HIV-1 Nef has been reported to disrupt MHC class II (MHCII)-mediated Ag presentation by a dual strategy that comprises a reduction in cell surface levels of peptide-loaded mature MHCII molecules and a up-regulation of immature MHCII molecules. We show that Nef achieves relocation of MHCII away from the cell surface in monocytic cells by both delaying its transport to the cell surface and by accelerating endocytic removal of cell surface MHCII to a lysosomal compartment. Nef-induced MHCII endocytosis is cholesterol-sensitive but clathrin- and dynamin-independent. Internalized MHCII molecules traverse the early endosomal system and colocalize with pinocytic cargo before reaching lysosomes. Nef-triggered MHCII endocytosis requires Rab5 activity and *lyst* function, whereas lysosomal trafficking of internalized MHCII molecules requires Rab7 activity. We further show that a similar pathway can remove peptide-MHCII complexes from the surface of monocytic cells not expressing Nef. Our data suggest that Nef uses mechanisms involved in normal MHCII recycling and turnover to mediate the delivery of cell surface MHCII to a lysosomal destination. Thus, Nef-mediated endocytosis of MHCII provides a novel perspective on the regulation of normal MHCII trafficking.   *The Journal of Immunology,* 2009, 183: 2415–2424.

The nonstructural Nef protein of HIV-1 is a critical contributor to viral pathogenicity in a variety of ways (1–4). Nef is a conglomerate of protein-protein interaction modules, intersecting multiple cellular trafficking, and signaling pathways (5, 6). Nef affects the expression of a variety of molecules on the APC surface that are critical in the generation of immune responses. Notably Nef mediates the down-regulation of cell surface levels of both classes of MHC molecules, as well as cell surface levels of the immune costimulatory molecules CD80 and CD86 (7–9).

Viruses that fuse at the plasma membrane and release most of their proteins directly into the cytosol, as well as viruses that establish persistent latent infections and constitutively express low levels of cytosolic Ags, have been found to be effectively detected by the presentation of cytosolic viral epitopes on MHC class II (MHCII)[4] (10). Viruses use multiple strategies to circumvent MHCII-dependent immunity, a common one being alteration in the cellular trafficking of MHCII (11). MHCII molecules extensively negotiate the endolysosomal system. Nascent MHCII molecules in complex with the invariant chain (Ii) exit the endoplasmic reticulum and move through the Golgi apparatus before intersecting the endocytic system in specialized MHCII peptide-loading compartments variously termed MIIC (MHCII-enriched compartment) or CIIV (class II vesicles) (12, 13). These compartments are thought to be a collection of late endocytic or lysosomal compartments containing the necessary components for Ii degradation and efficient peptide loading on MHCII before its egress to the cell surface (13, 14). Constitutive endocytosis and recycling of cell surface MHCII have also been well documented (15) and are considered a pathway for the presentation of some Ags (16), although the molecular regulators of such trafficking are not yet well understood. The extensive dependence of MHCII on the endocytic system for its function offers a potential target for viral subversion.

Nef has been reported to inhibit MHCII-dependent Ag presentation by the reduction of cell surface levels of mature MHCII and the up-regulation of immature MHCII, which are functionally incompetent because of persistent association with the Ii (9). In the presence of Nef, mature MHCII molecules are reduced at the cell surface and are found at high levels in intracellular lysosomal compartments. The delivery of immature MHCII to the endolysosomal compartment is also impaired, resulting in reduced Ii degradation (17). Mutational analysis suggests that these mechanisms are well conserved among *nef* alleles (18).

Endocytic mechanisms involve a variety of internalization pathways with variable dependence on factors such as coat proteins like clathrin and caveolin, levels of membrane cholesterol, and scissoring agents such as dynamin (Dyn) and small GTPases of the Rho family (19, 20). This potentially provides Nef with an assortment of molecular adaptors that can be subverted. Nef is known to affect many of these endocytic programs to modulate the expression of several cell surface molecules (4).

On this background, we have examined the process by which Nef mediates the redistribution of MHCII in human monocytic

*National Institute of Immunology, New Delhi, India; [†]International Centre for Genetic Engineering and Biotechnology, New Delhi, India; and [‡]National Centre for Biological Sciences, Bangalore, India

cells. We find that Nef triggers MHCII internalization in a cholesterol-dependent but clathrin- and Dyn-independent manner that closely mimics the constitutive endocytosis of peptide-MHCII molecules. These findings indicate that Nef exploits a constitutive endocytic program to subvert surface MHCII expression in HIV-infected cells.

Materials and Methods

Plasmids and reagents

The *F2-nef* gene from an Indian HIV-1 subtype C primary isolate cloned into pIRES2-EGFP or pEGFP-N3 has been described earlier (7). The K44A dominant negative (DN)-Dyn construct was obtained from Dr. M. McNiven (Mayo Clinic, Rochester, MN), the DN Eps15 construct from Dr. A. Dautry-Varsat (Institut Pasteur, Paris, France), the Rab11 constructs from Dr. N. Bunnett (University of California, San Francisco, CA), and the Rab5- and Rab7-related constructs from Dr. M. Zerial (Max Planck Institute of Molecular Cell Biology and Genetics, Dresden, Germany) for use as described earlier (21).

The following reagents were used: fluorophore-labeled dextran (tetramethylrhodamine-dextran) and transferrin (Tf) (Molecular Probes), mAbs against Rab5, Rab11, EEA1, LAMP1 (Transduction Laboratories), and Rab7 (Santa Cruz Biotechnology), anti-human MHCII (L243) either purified from culture supernatants or used as a biotin conjugate (Serotec), and purified anti-MHCII mAb labeled with either Cy5 (Amersham), or with Alexa Fluor dyes (Molecular Probes). The mAbs Y-Ae (anti-Ea$_{52-68}$-H-2A^b) and Y3P (anti-H-2A^b) have been described previously (22). Labeled secondary detection reagents used included goat anti-mouse IgG (Fc)-PE, donkey anti-rat IgG (Fc)-PE (Jackson ImmunoResearch Laboratories), streptavidin-PE, streptavidin-CyChrome, and streptavidin-PE-Texas Red (BD PharMingen).

Cells and transfection

BMC-2 cells were maintained in Click's medium with FCS, 2-ME, L-glutamine, and antibiotics. U937 cells were maintained in RPMI 1640 medium with FCS and antibiotics. Cells were kept in 0.5 μg/ml LPS overnight before use to enhance MHC levels. Primary murine monocytes were grown from mouse bone marrow by culturing nonadherent mouse bone marrow cells with M-CSF (30% L929 fibroblast-conditioned medium as M-CSF source) for 7 days, with periodic growth factor replenishment. Primary human monocytes were grown from PBMC by culturing them with rM-CSF (100 U/ml; Sigma-Aldrich) for 3 days, and live cells were used for infection in the continuing presence of the growth factor. Transfections of cell lines and mouse primary cells were done using FuGENE 6 (Roche) or Effectene (Qiagen), according to the manufacturers' protocols. Primary human monocytes were transfected by nucleoporation according to the manufacturer's protocol (Amaxa). Briefly, 1×10^6 cells were resuspended in Nucleofector solution followed by the addition of 4–6 μg of plasmid DNA and cells were nucleoporated following manufacturer's instructions (Amaxa).

Antigens

A recombinant fusion protein (GST-Ea$_{52-68}$-Myc) consisting of GST, aa residues 52–68 of the mouse H-2Ea sequence (Ea$_{52-68}$), and the oligopeptide sequence of the c-Myc protein was made in *Escherichia coli* from the plasmid pGEX-2T as described previously (22).

Immunofluorescence microscopy and image processing

Cells were fixed with 4% paraformaldehyde for 20 min at 37°C and permeabilized using 0.3% Tween 20 or 0.03% saponin in PBS for 20 min at ambient temperature. They were then blocked with 2 mg/ml BSA in PBS before incubation with Abs in the same medium. Rabbit and mouse primary Abs were detected using fluorophore-labeled, Fc-specific anti-rabbit IgG or anti-mouse IgG.

Confocal and wide field microscopy

Confocal imaging was conducted on a Zeiss LSM510 confocal microscope (Zeiss) equipped with factory set dichroics and an argon-krypton laser using the Zeiss software with a step size of 0.1 μm and a digital zoom of 3.5 corresponding to a pixel size of 0.10 μm was used. Pinhole size was kept constant at 272 U (optical section, <2 μm; airy units, <3), and 12 bit images were collected at ×63 original magnification and a 1.45 numerical aperture (NA) objective.

Optimized dichroics, excitation, and emission filters were used as described (23). Fluorophores were imaged for multiwavelength analysis us-

ing appropriate filter sets. For four-color imaging, either factory-set dichroics (Zeiss) or spectral separation by the 32-channel Meta detector (Zeiss) with dye-specific laser line excitation was used. The absence of cross-excitation was confirmed in both approaches (data not shown).

High-resolution, wide-field images were collected using Nikon TE 300 inverted microscope equipped with ×60 original magnification/1.4 NA objective and ×20 original magnification/0.75 nuclear NA, a mercury arc illuminator (Nikon), and a cooled charge-coupled device camera (Princeton Instruments) controlled by Metamorph software (Molecular Devices).

Quantitative colocalization analysis

Colocalization between internalized vesicles and endocytic markers was quantified using two types of software, MultiSpots and MultiColloc (21, 24), variations of the custom-developed software, Spots and Coloc, respectively, as described previously (21, 25–28). The criteria outlined below were applied to images obtained from U937 cells labeled with Abs against Rab5, EEA1, Rab7, Rab11, and LAMP1 or pulsed with the endocytic tracers Tf and dextran for 10 min at 37°C. High-resolution images of cells labeled with endocytic tracers were obtained using a ×60 original magnification, 1.4 NA objective on a wide-field microscope at a pixel resolution of 0.15um/pixel. The images were corrected for background fluorescence using the "produce background correction" image procedure in Metamorph image analysis software with the following parameters suitable for producing a local background image while at the same time preserving the intensity of the endosomes (box size, 30 × 30 pixels; subsample ratio, 10; percentile, 0.2).

The background corrected images were then processed through Multi-Spots to identify endosomes using parameters defined by pixels above a threshold (set by inspection for each image) and area (minimum, 3 pixel; maximum, no upper limit). A trimming procedure was applied to isolate and segregate individual endosomes based on the inclusion of pixels with intensities >0.3 of maximal intensity within a unit of connected pixels having an intensity greater than that of the set threshold. This was achieved by an iterative procedure using a step size (0.01) for each iteration with limits for the number of iterations of the trimming procedure. The resultant image contains a set of identified "spots or endosomes" quantified in terms of net intensity per spot and total pixel area per spot.

The two "spotted" images of different fluorophore-labeled markers were matched up against each other to identify the endosomes wherein the two molecules were colocalized. Endosomes in a tracer image (e.g., MHCII-associated endosomes) were compared with endosomes in a reference image (e.g., Rab11-containing endosomes) using MultiColoc, and endosomes with ≥50% area overlap were considered to be colocalized. The resultant image displayed all of the spots that were colocalized using a particular "tracer-reference" image pair.

Cell outlines were drawn based on the phase contrast image of the cell, and the net intensity of each fluorophore per cell was calculated in the spotted as well as the colocalized images using procedures in Metamorph. The percentage of colocalization was then calculated from the ratio of the net intensity within a cell in the MHCII with the appropriate Rab5/EEA1/Rab11/etc-endocytic marker MultiColoc image to the net intensity of the same cell in the MHCII spots image. The maximum extent of colocalization obtained by this method is 90% for the colocalization of cointernalized Alexa Fluor 568-Tf and Alexa Fluor 647-Tf in the same cell. The percentage of colocalization is represented as a mean and SEM obtained from three independent experiments with a minimum of 50 cells per experiment. All images were processed for output purposes using Adobe Photoshop software. Digital color assignments were made for each fluorophore so as to provide maximum visual contrast.

Cell labeling and other treatments

U937 cells were transfected with various plasmids and surface labeled 12 h later with either biotinylated or primary-labeled anti-MHCII Ab on ice for 30 min. Cells were then warmed to 37°C and chased for varying lengths of time.

To visualize the endosomal distribution of the fluorescent tracers, the cell surface label (fluorophore-labeled Tf or anti-MHCII) was removed by using a combination of low pH and high pH buffers (ascorbate buffer (pH 4.5),160 mM sodium ascorbate, 40 mM ascorbic acid, 1 mM MgCl$_2$, and 1 mM CaCl$_2$).

Flow cytometry

Cells were stained with primary and secondary reagents on ice for 30 min, as appropriate. For intracellular staining, cells were permeabilized with 0.03% saponin. Stained cells were analyzed on a BD-LSR flow cytometer (BD Biosciences) and data were analyzed using FlowJo software (Tree Star). All data shown are representative of 3–5 independent experiments.
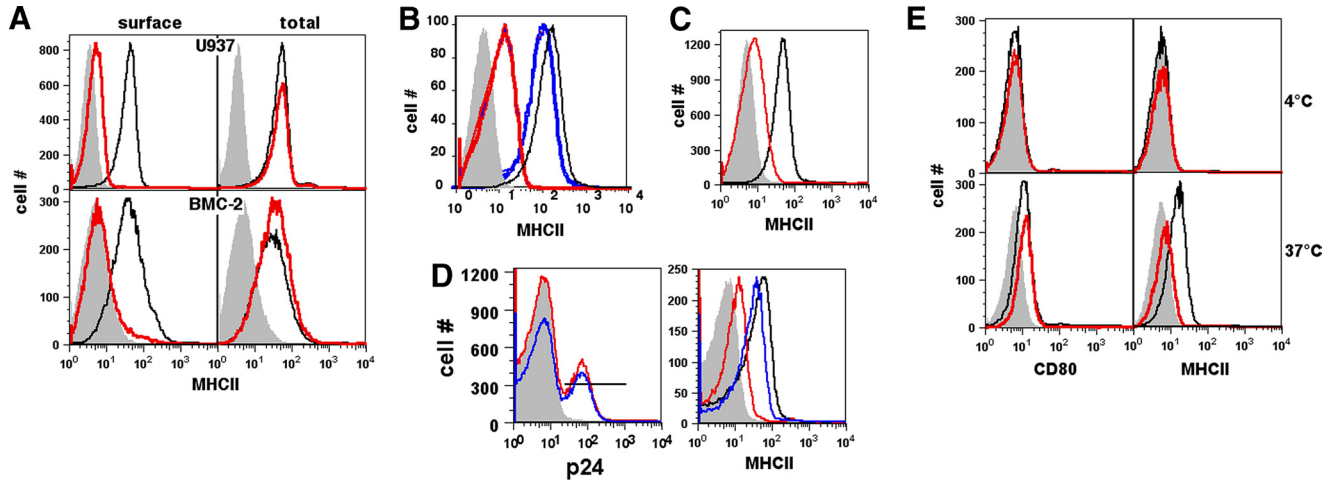
FIGURE 1. HIV-1 Nef reduces cell surface but not total MHCII levels on human and mouse myeloid cells. *A*, U937 or BMC-2 cells were transfected to express either eGFP alone (black lines) or Nef and eGFP (red lines) and stained 24 h later for MHCII either before (surface) or after (total) permeabilization. Histograms show MHCII levels on eGFP-gated cells. *B*, U937 cells were either mock infected (black line) or infected with WT HIV-1 (NL4-3; blue line) or with *nef*-deleted NL4-3 virus (red line) and stained for cell surface MHCII and intracellular HIV-1 p24 protein 2 days later. Histograms show surface MHCII levels on p24-gated cells. *C*, Primary human monocytes were transfected to express either eGFP alone (black lines) or Nef and eGFP (blue lines) and stained 24 h later for cell surface MHCII. Histograms show MHCII levels on eGFP-gated cells. *D*, Primary human monocytes were either mock infected (black line) or infected with WT HIV-1 (NL4-3 Ada; red line) or *nef*-deleted NL4-3 Ada virus (blue line) and stained for cell surface MHCII and intracellular HIV-1 p24 protein 2 days later. Histograms in the *left panel* show p24 levels in infected cells and the p24 gate used. Histograms in the *right panel* show surface MHCII levels on p24-gated cells. *E*, U937 cells transfected to express either eGFP alone (black lines) or Nef and eGFP (red lines) were stained 12 h after transfection with anti-MHCII-biotin or anti-CD80-biotin, and held at either 4°C or 37°C as indicated. Cells were then stained with the same anti-MHCII or anti-CD80 mAbs conjugated to PE to detect newly expressed molecules. Histograms show levels of new MHCII or CD80 molecules delivered to the cell surface as detected by PE-labeled mAbs in eGFP-gated cells. Gray curves in all panels represent isotype controls. Data are representative of 3–5 independent experiments.

Viruses and infection

HIV-1 viral stocks were generated by electroporation of HeLa cells with the infectious molecular clones pNL4-3 and pNL4-3 FS Nef (gifts from H. Gottlinger, University of Massachusetts Medical School, Worcester, MA) or pNL4-3 ADA and pNL4-3 ADAΔNef (gifts from M. Stevenson, University of Massachusetts Medical School, Worcester, MA). Virus stocks were harvested 72 h later and filter sterilized. U937 cells or primary human monocytes were serum starved for 1 h before infection. For each infection, 1×10^6 cells were infected with 100,000–200,000 cpm of reverse-transcriptase counts of virus. After 4 h of adsorption, cells were washed and incubated for 48 h before being stained for surface MHCII and intracellular p24 Gag protein.

Animals

C57BL/6 and *bg/bg* mice were obtained from The Jackson Laboratory and bred in the small animal facility of the National Institute of Immunology (New Delhi, India). All animal experiments were done under the approval of the Institutional Animal Ethics Committee.

Results

HIV-1 Nef reduces cell surface MHCII levels in myeloid cells

A wild-type (WT) *nef* gene (F2-*nef*) cloned from an Indian clinical isolate (7) was transfected into the human monocytic U937 cell line. Cell surface MHCII levels were reduced 5- to 10-fold at 48 h post-transfection (Fig. 1*A*). This was accompanied by a reduction in the levels of MHC class I (MHCI), CD80, and CD86 as reported earlier (7), whereas levels of other molecules such as the Tf receptor did not exhibit any changes (Ref. 7 and data not shown). The total cellular levels of MHCII, however, as measured by staining postpermeabilization, were unaltered (Fig. 1*A*). Furthermore, Nef expression led to a similar reduction of cell surface MHCII levels in the murine monocytic cell line BMC-2, although there was no reduction in the total cellular levels of MHCII postpermeabilization (Fig. 1*A*). Similar effects were found on primary mouse bone marrow-derived dendritic cells and monocytes as well (data not shown). MHCII levels were also dramatically reduced on U937

monocytic cells infected with WT HIV-1, in contrast to cells infected with Nef-deficient HIV-1 (Fig. 1*B*). The modest residual reduction in surface MHCII levels in the cells infected with Nef-deficient HIV-1 could be the effect of the Vpu protein of HIV-1, which has previously been shown to cause such a modest reduction in cell surface MHCII levels in monocytic cells (29).

We next tested whether the reduction of cell surface MHCII levels observed in Nef-expressing U937 cells or in mouse monocytic cells was also observed in primary human monocytes. Human primary monocyte cultures were transfected to express enhanced GFP (eGFP) alone or Nef and eGFP. Expression of Nef in human primary monocytes also led to a reduction in cell surface MHCII levels (Fig. 1*C*). We also confirmed that the infection of primary human monocytes with WT HIV-1 (Ada strain) led to substantial loss of cell surface MHCII levels, whereas infection with Nef-deleted HIV-1 (Ada) did so only modestly (Fig. 1*D*, *right panel*). It is noteworthy that, under the conditions used, the two viruses did not show notable differences in their ability to infect primary human monocytes (Fig. 1*D*, *left panel*). Thus, a reduction in cell surface MHCII levels by Nef is relevant for the human monocytic lineage.

To further characterize Nef-mediated down-modulation of MHCII in monocytic cells, we tested some Nef mutants we have previously reported on for their effects on MHCI down-modulation in myeloid cells, using either the human cell line U937 and/or the mouse cell line BMC-2. All findings were consistent between the two cell lines. As expected, the GG to AA mutation of Nef at residues 2 and 3 (G2A), known to be deficient in myristoylation, was unable to down-regulate MHCI or MHCII (Table I). Deletion mutants of Nef truncated from the C terminus to residue 130 continued to show efficient down-modulation of MHCI and MHCII, and while further deletion to residue 105 led to a loss of MHCI down-modulation, this mutant continued to down-modulate MHCII. However, a further deletion to residue 78 led to a loss of

Table I. *Effects of Nef mutations on Nef-mediated down-modulation of cell surface MHCII in monocytic cell lines*

Mutants	U937 Human Cells[a]		BMC-2 Mouse Cells[a]	
	MHCI[b]	MHCII	MHCI[b]	MHCII
F2-*nef* (WT)	+	+	+	+
F2-*nef*-G2A	−	−	−	−
F2-*nef*-Δ78	−	−	−	−
F2-*nef*-Δ105	−	(+)	−	(+)
F2-*nef*-Δ125	(+)	(+)	(+)	(+)
D1-*nef*	−	(+)	−	(+)

[a] +, Persistence of down-modulation ability; −, loss of down-modulation ability; (+), weak persistence of down-modulation.
[b] MHCI-related data from Ref. 7.

down-modulation of both MHCI and MHCII (Table I). A clinical isolate of Nef mutated in both the WL57 site and the phosphofurin acidic cluster-sorting protein (PACS)-binding E4 site (D1-Nef) (7) also showed a loss of MHCI- and MHCII-down-modulation activity (Table I).

Nef retards the delivery of MHCII molecules to the plasma membrane

Previous reports regarding the effects of Nef on cell surface MHCII levels could be interpreted to imply that Nef reduces the rate of MHCII delivery to the cell surface as well as accelerating the removal of cell surface MHCII molecules. We tested both of these possibilities. To test the effect of Nef on the delivery of intracellular MHCII to the cell surface, Nef-expressing U937 cells were stained 12 h after transfection with biotinylated anti-MHCII or anti-CD80 mAbs. They were then either held at 4°C or cultured at 37°C for 2 h. The cells were then stained with Cy3-streptavidin to detect the prelabeled molecules, as well as with the same anti-MHCII or anti-CD80 mAbs conjugated to PE to detect newly expressed molecules. Because the cell surface MHCII and CD80 were saturated with the first round of mAb binding, no staining was seen with the second round PE-labeled mAbs when the cells had been held at 4°C, showing that no new MHCII or CD80 molecules had arrived at the surface (Fig. 1E). However, if the cells were held at 37°C for 2 h, unlabeled CD80 appeared on the surface and the extent of expression of unlabeled CD80 was not different between eGFP-expressing or Nef-eGFP-expressing cells, indicating that Nef did not affect the rate of exocytosis of CD80 molecules to the cell membrane. In contrast, whereas newly delivered MHCII molecules could indeed be detected in cells held at 37°C, their levels were lower in Nef-expressing cells (Fig. 1E), indicating that Nef retards the delivery of intracellular MHCII molecules to the cell surface.

Nef relocates cell surface MHCII to intracellular lysosomal compartments

Nef-mediated internalization of cell surface MHCII was next tracked by the disappearance of MHCII from the cell surface over time in eGFP- or Nef-expressing U937 cells, by labeling surface MHCII with biotinylated mAb and chasing for various times before flow cytometric estimation of surface label loss with fluorophore-labeled streptavidin. To confirm that the label lost from the surface was retained intracellularly, cells were also permeabilized and stained at each chase time point. The data show that in the absence of Nef, MHCII resides stably at the cell surface over an 8-h period, whereas in the presence of Nef MHCII was progressively lost from the surface but re-
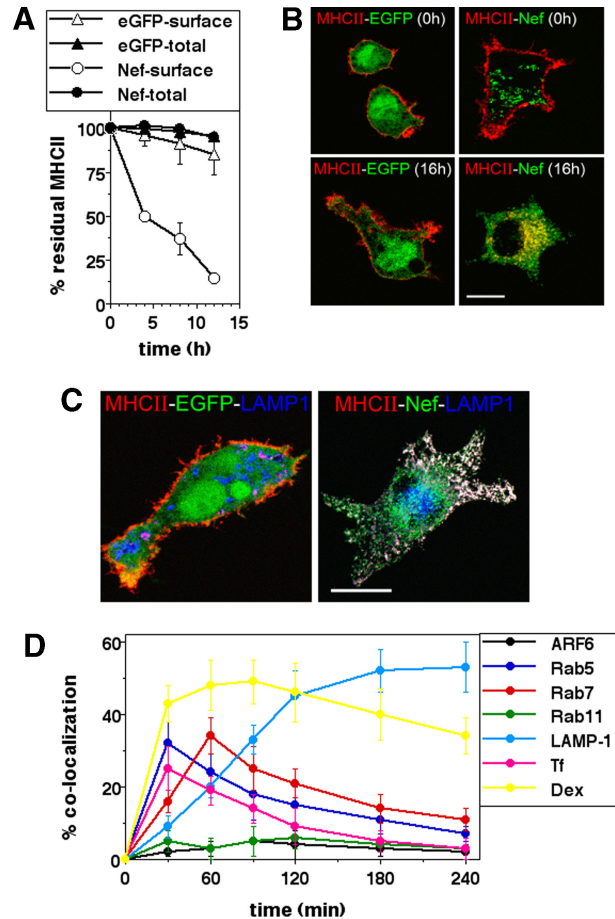
FIGURE 2. Nef traffics cell surface MHCII to lysosomal compartments. *A,* U937 cells transfected to express either GFP alone or Nef and eGFP as indicated were surface labeled with anti-MHCII-biotin 12 h after transfection and then cultured for various times as indicated and subjected to the detection of either surface (open symbols) or total (closed symbols) label postpermeabilization. Mean fluorescence intensities were calculated for eGFP-gated cells and the data normalized to the starting intensities as a percentage of the residue of surface-labeled MHCII. The graphs show mean ± SD values of detected fluorescence label calculated from three independent experiments. *B,* U937 cells transfected to express eGFP (*left column*) or Nef-eGFP (*right column*) were surface-labeled 12 h later with anti-MHCII-biotin, and were either stained with labeled streptavidin-Alexa Fluor 568 immediately (0 h; *top row*) or cultured for 16 h before staining (16 h; bottom row), followed by confocal microscopic imaging. Scale bar, 10 μm. *C,* U937 cells transfected to express eGFP (*left*) or Nef-eGFP (*right*) were fixed 24 h after transfection and stained for MHCII (red; Alexa Fluor 568) and LAMP-1 (blue; Alexa Fluor 647), followed by confocal microscopy. Scale bar, 10 μm. *D,* U937 cells expressing Nef-eGFP were labeled for MHCII at the cell surface and cultured for various times as indicated. At each time point shown the surface label was stripped and cells were permeabilized and stained for the vesicular marker indicated. For detection of Arf6, U937 cells were cotransfected with plasmids expressing Nef-HA and Arf6-eGFP, and staining include hemagglutinin epitope detection. For tracking colocalization with dextran (Dex) or Tf, cells were given a 10-min pulse with fluorophores, Alexa Fluor 568-Tf or tetramethylrhodamine-Dex 3 h after surface labeling for MHCII. Cells were imaged by either high-resolution, wide-field fluorescence microscopy or confocal microscopy. Images of Nef-expressing cells were quantified for the fraction of internalized MHCII colocalizing with the various markers shown. Data are plotted as the extent of colocalization over time (mean ± SE; n = 100 cells).

mained detectable intracellularly (Fig. 2A). We also tracked the internalization of cell surface MHCII molecules by labeling Nef-transfected U937 cells with fluorochrome-tagged

anti-MHCII Ab, followed by confocal microscopic examination over time. By 16 h after surface labeling, MHCII molecules had disappeared from the surface of Nef-expressing, but not from control eGFP-expressing U937 cells, and were relocated in intracellular compartments (Fig. 2*B*).

To identify the intracellular compartment where MHCII was located in Nef-expressing cells, we examined Nef-eGFP-expressing U937 cells for colocalization of MHCII with markers of intracellular compartments by confocal microscopy. Nef-eGFP was colocalized with endogenous MHCII in intracellular organelles marked by the lysosomal marker LAMP-1 (Fig. 2*C*). Although almost all cell surface MHCII was relocated under the influence of Nef into some LAMP-1-marked compartments, LAMP-1-marked compartments not containing MHCII could also be detected (Fig. 2*C*), indicating that Nef induced MHCII relocation to specific vesicles within LAMP-1-marked regions.

Nef redistributes surface MHCII to the lysosomal compartment via endosomal vesicles

We next examined the colocalization of internalized MHCII in Nef-expressing cells with a range of vesicular and endosomal markers at intermediate stages of internalization to track the pathway of internalization (Fig. 2*D*). Internalized MHCII molecules in Nef-expressing cells initially colocalized in vesicles bearing Rab5. If the cells were pulsed with either Tf or a fluid-phase marker, tetramethylrhodamine-dextran at appropriate times, initial colocalization was seen with both markers; but whereas Tf was rapidly sorted away from the MHCII, dextran showed stable colocalization. As MHCII-carrying endosomes lost Rab5, they moved into Rab7-bearing compartments from where they began to accumulate stably in LAMP-1-bearing vesicles. No colocalization was seen with either Arf6 or Rab11. These results suggest that, under the influence of Nef, MHCII traffics from early endosomal compartments to lysosomes along with fluid-phase cargo via late endosomal compartments, following the classical pathway of postendocytotic progression.

Molecular mediators of Nef-induced MHCII endocytosis

We next attempted to identify the molecular intermediates critical for Nef-mediated endocytosis of cell surface MHCII. Because Nef induces both an exocytic blockade and an enhanced endocytosis of MHCII, we distinguished between these two processes in many of the following experiments by using the methodology described above, namely labeling surface MHCII with biotinylated mAb and chasing for various times before flow cytometric estimation of surface label loss with fluorophore-labeled streptavidin. However, detection of cellular levels of MHCII without prior labeling also gave similar results in all instances.

Because MHCII molecules that are being internalized under the influence of Nef first enter compartments marked by the small GTPase Rab5, we examined whether Rab5 was involved in the process of removal. For this, U937 cells were cotransfected with Nef and either WT Rab5 or a DN mutant (S34N) (30) version of Rab5. Cells were stained 36 h later for cell surface MHCII or MHCI. In cells coexpressing Nef with DN Rab5, MHCII internalization was notably reduced whereas MHCI relocation was not blocked (Fig. 3*A*). Similar data were obtained when cell surface MHCII molecules were prelabeled and chased. The removal of prelabeled MHCII from the surface of Nef-expressing U937 cells was retarded by DN Rab5, and was accelerated by a constitutively active (CA) (30) mutant (Q79L) of Rab5 (Fig. 3*B*). These data thus implicated Rab5 in the Nef-mediated removal of cell surface MHCII and indicated a difference between the mechanisms of Nef-induced trafficking of cell surface MHCI and MHCII.
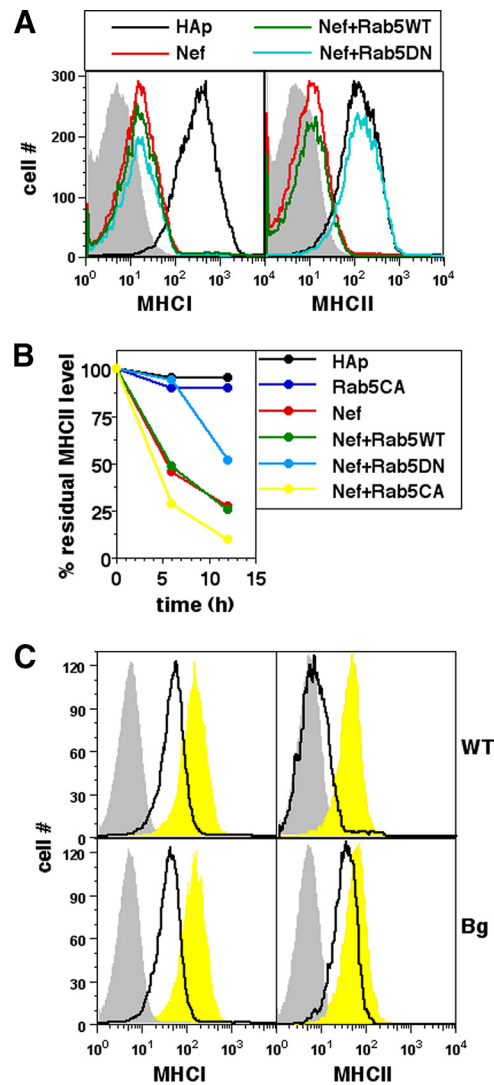
FIGURE 3. Nef-mediated removal of cell surface MHCII requires Rab5 and Lyst. *A*, U937 cells were either singly transfected or cotransfected for expression of hemagglutinin epitope (HAp) alone or F2-Nef-HAp and WT Rab5 or DN Rab5 in combinations as indicated. Cells were stained for cell surface MHCI or MHCII 24 h later and analyzed by flow cytometry. Single-color histograms show surface MHCI or MHCII levels on HAp-gated cells. Isotype controls are shown as gray-shaded curves. *B*, U937 cells were either singly transfected or cotransfected for expression of HAp alone or F2-Nef-HAp and WT Rab5, CA Rab5, or DN Rab5 in combinations as indicated. Cells were stained with anti-MHCII-biotin 12 h later and cultured for various times as shown before detection of the residual cell surface label. Mean fluorescence intensities were calculated for HAp-gated cells and the data were normalized to the starting intensities as a percentage of the residue of surface-labeled MHCII as shown. *C*, BMDMs derived from WT C57BL/6 or *bg/bg* (Bg) mice were transfected to express either eGFP alone (yellow curves) or Nef and GFP (black lines) and stained for cell surface MHCI or MHCII 24 h later for analysis by flow cytometry. Single-color histograms show surface MHCI or MHCII levels on eGFP-gated cells. Isotype controls are shown as gray-shaded curves.

As shown above, Nef-mediated endocytosis of surface MHCII was followed by their delivery from early Rab5-bearing endosomes to late Rab7-bearing endosomes. A protein encoded by the *lyst* gene is known to modulate this trafficking. The beige mouse strain (Bg) harbors a mutation in the *lyst* gene and its cells show reduced sorting to late endosomal compartments (31). Because Nef had similar effects on the removal of surface MHCI and MHCII in
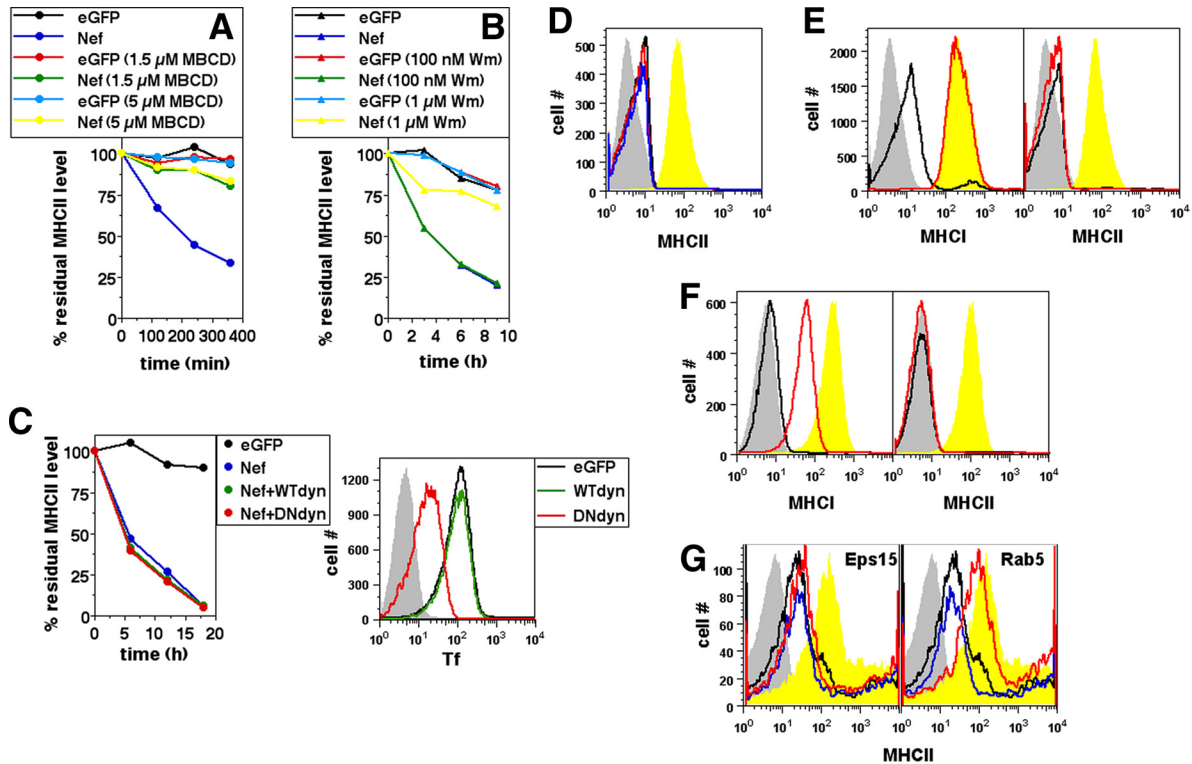
FIGURE 4. Nef-mediated removal of cell surface MHCII is dependent on cholesterol and PIK but is independent of Dyn, Eps15, or intersectin. *A* and *B*, U937 cells transfected to express either eGFP alone or Nef and GFP were cultured in the presence or absence of various concentrations of MBCD (*A*) or Wm (*B*) as indicated. Cells were stained with anti-MHCII 12 h later and cultured for various times as shown before detection of the residual cell surface label. Mean fluorescence intensities were calculated for eGFP-gated cells and the data normalized to the starting intensities as a percentage of the residue of surface-labeled MHCII as shown. *C*, U937 cells were transfected to express either eGFP or Nef and GFP and WT Dyn or DN Dyn as shown. Cells were stained with anti-MHCII 12 h after transfection and cultured for various times as shown before detection of the residual cell surface label. Mean fluorescence intensities were calculated for eGFP-gated cells and the data normalized to the starting intensities as a percentage of the residue of surface-labeled MHCII as shown (*left panel*). *Right panel* shows U937 cells transfected to express eGFP alone or with either WT Dyn or DN Dyn as indicated and given a 10-min pulse with fluorophore-labeled Tf 3 h before staining. Histograms show Tf uptake levels in eGFP-gated cells. Gray curves indicate isotype controls. *D*, U937 cells were transfected to express either eGFP alone (yellow curves) or Nef-positive GFP alone (black line) or with either control plasmid (blue line) or sh-Dyn (red line). Cells were stained 24 h later for MHCII. Histograms show surface MHCII levels on eGFP-gated cells. Gray curves indicate isotype controls. *E* and *F*, U937 cells were transfected to express either eGFP alone (yellow curves) or Nef and GFP alone (black line) or with DN eps15 (red line; *E*) or intersectin-A (red line; *F*). Cells were stained 24 h later for cell surface MHCI or MHCII. Histograms show surface MHCI and MHCII levels on eGFP-gated cells. Gray curves indicate isotype controls. *G*, Human primary monocytes were either untransfected (yellow curves) or transfected to express Nef by itself (black line) or along with either WT Eps15 (*left panel*; blue line) or DN Eps-15 (*left panel*; red line) or WT Rab5 (*right panel*; blue line) or DN Rab5 (*right panel*, red line). Cells were stained 24 h later for MHCII. Histograms show surface MHCII levels on cells gated for expression of transfected gene/s. Gray curves indicate isotype controls.

mouse myeloid cells (Ref. 7 and data above), we used bone marrow-derived monocytes (BMDMs) grown from either WT or Bg mice and transfected to achieve Nef expression. Nef-expressing Bg BMDMs showed reduced loss of surface MHCII although MHCI relocation was unaffected (Fig. 3*C*), again indicating that Nef-mediated removal of MHCII was dependent on the endocytotic trafficking pathway from early to late endosomes.

We (24) and others (32) have previously reported that MHCI removal from the cell surface in Nef-expressing cells is dependent on cholesterol and phosphatidylinositol kinase (PIK) activity. We therefore tested whether MHCII removal in Nef-expressing cells was similarly controlled. Cellular cholesterol was depleted in U937 cells using the cholesterol-chelating agent methyl-β-cyclodextrin (MBCD). MHCII removal from the cell surface was sensitive to MBCD (Fig. 4*A*) like MHCI removal (24). Low concentrations of wortmannin (Wm), a PIK inhibitor reported to be specific for PI3K (33), did not affect Nef-mediated removal of MHCII whereas a higher concentration retarded it (Fig. 4*B*), similar to the finding for MHCI removal (24).

Although Nef-mediated CD4 internalization is Dyn dependent, that of MHCI, CD80, or CD86 is not (34). We therefore tested the effect of the DN K44N mutant of Dyn-2 (DN Dyn) (35) or that of a short interfering RNA for Dyn-2 (sh-Dyn) (36) on Nef-mediated MHCII down-modulation in Nef-expressing U937 cells. DN Dyn had no effect on Nef-induced loss of cell surface MHCII (Fig. 4*C*) or MHCI, CD80, or CD86 as reported earlier (24), although Dyn-dependent Tf endocytosis was blocked as expected (Fig. 4*C*). Similarly, sh-Dyn did not have any effect on the Nef-induced removal of cell surface MHCII (Fig. 4*D*). DN versions of other GTPases known to be involved in many endocytotic pathways, such as Rho or Cdc42, did not have any effects on the removal of either MHCII or MHCI in Nef-expressing cells (data not shown). Furthermore, the blockade of molecular activities known to be crucial for the removal of the costimulatory molecules CD80 and CD86 from the surface of Nef-expressing myeloid cells, such as Rac, WASP, TIAM, Src, protein kinase C, or actin (24), had no effect on the reduction of surface MHCII levels in Nef-expressing cells (data not shown).

To assess the role of clathrin in Nef-induced MHCII internalization, U937 cells were cotransfected with Nef and either a DN version of the clathrin adaptor protein Eps15 (95/295) (37) or a DN fragment of another adaptor protein, intersectin (intersectin-A) (38). DN Eps-15 and intersectin-A blocked the uptake of Tf as expected (data not shown). In cells coexpressing Nef with DN Eps15 or intersectin-A, MHCII internalization was unaffected while MHCI relocation was blocked (Figs. 4, E and F), identifying another difference between the Nef-induced trafficking pathways for MHCI and MHCII.

Together, these data indicate that although mechanisms for cell surface MHCI and MHCII removal in Nef-expressing cells have some similarities, they differ in their entry into Tf- and fluid phase-marked compartments and in their dependence on clathrin complexes vs Rab5 and Lyst activity.

We also confirmed that the role for Rab5 and the lack of a role for Eps15 in Nef-mediated relocation of MHCII was relevant in primary human monocytes as well. Human primary monocyte cultures were cotransfected to express Nef with either WT Rab5/DN Rab5 or WT Eps15/DN Eps15 as above and stained to assess surface MHCII levels. DN Rab5 blocked Nef-mediated relocation of MHCII whereas DN Eps15 did not (Fig. 4G), confirming that the observations on U937 cells were consistent with those on primary human monocytes.

Cell surface MHCII was sorted to LAMP-1-bearing compartments via Rab7-bearing vesicles in Nef-expressing cells as shown above. The endocytosis of MHCII from the surface in Nef-expressing cells appears to be controlled by Rab5 and Lyst. We therefore examined whether Rab7 was crucial in mediating the Nef-mediated lysosomal delivery of MHCII. U937 cells were cotransfected with Nef and a DN mutant (N125I) version of Rab7. DN Rab7 did not block removal of cell surface MHCII (Fig. 5A). However, although internalized MHCII was relocated to LAMP-1-bearing compartments in Nef-expressing cells carrying WT Rab7, this colocalization was blocked in DN Rab7-expressing cells (Figs. 5, B and C), demonstrating that Rab7 is critical for lysosomal delivery of internalized MHCII.

Endocytic intermediates involved in constitutive turnover of peptide-MHCII complexes

The data above indicated that Nef-mediated endocytotic removal of cell surface MHCII in both human and mouse myeloid cells was initiated by cholesterol- and PIK-dependent events requiring both Rab5 and Lyst. We next examined whether Nef assembled this de novo pathway for MHCII internalization or whether it subverted an existing pathway in the constitutive turnover of MHCII molecules. For this purpose, we generated specific peptide-MHCII (pMHCII) complexes on the surface of the mouse monocytic cell line BMC-2 and tracked its fate using a mAb specific for this pMHCII complex. A peptide from the endogenous protein H-2E-α (Ea52–68; Eap) binds with high affinity to the H-2A^b MHCII molecule, and this pMHCII complex is specifically recognized by the Y-Ae mAb (39). Therefore, cell surface pMHCII complexes were generated by pulsing BMC-2 cells with synthetic Eap for 60 min. Pulsed cells were incubated for varying times before being stained with either the pMHCII-specific mAb Y-Ae or the H-2A^b-specific mAb Y-3P for flow cytometry (Fig. 6A) or were labeled at 4°C with biotinylated Y-Ae or Y-3P and then incubated for varying times at 37°C followed by flow cytometric detection using fluorochrome-coupled streptavidin (Fig. 6B). Y-Ae-binding pMHCII complexes generated on BMC-2 cells were lost rapidly from the cell surface, whereas the total H-2A^b levels did not show any notable change (Figs. 6, A and B). We then examined whether the molecular intermediates involved in Nef-mediated removal of cell
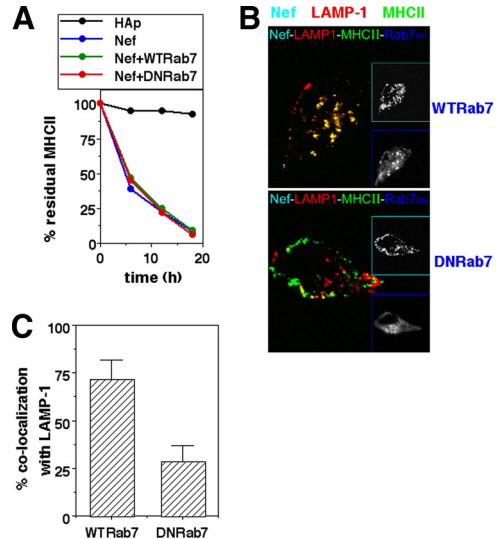
FIGURE 5. Rab7 is required for lysosomal delivery of MHCII removed from the surface in Nef-expressing cells. *A*, U937 cells were either singly transfected or cotransfected for expression of hemagglutinin epitope (HAp) alone or F2-Nef-HAp or WT Rab7 or DN Rab7 in combinations as indicated. Cells were stained with anti-MHCII-biotin 12 h later and cultured for various times as shown before the detection of residual cell surface label. Mean fluorescence intensities were calculated for HAp-gated cells and the data normalized to the starting intensities as a percentage of the residue of surface-labeled MHCII. *B*, U937 cells transfected to express Nef-GFP with either WT Rab7 or DN Rab7-eGFP (blue) were fixed 24 h after transfection and stained for MHCII (green; Alexa Fluor 647) and LAMP-1 (red; Alexa Fluor 568) followed by confocal microscopy. *Inset*s show gray-scale images of the same cells for cyan and blue colors as identified by the *inset* frames. *C*, Nef-HAp-expressing cells from the experiment shown in *B* above were quantified for the fraction of internalized MHCII colocalizing with LAMP-1 in the presence of WT Rab7 or DN Rab7 (mean + SE; *n* = 50 cells).

surface MHCII also regulated the specific loss of Y-Ae-binding pMHCII complexes from the cell surface.
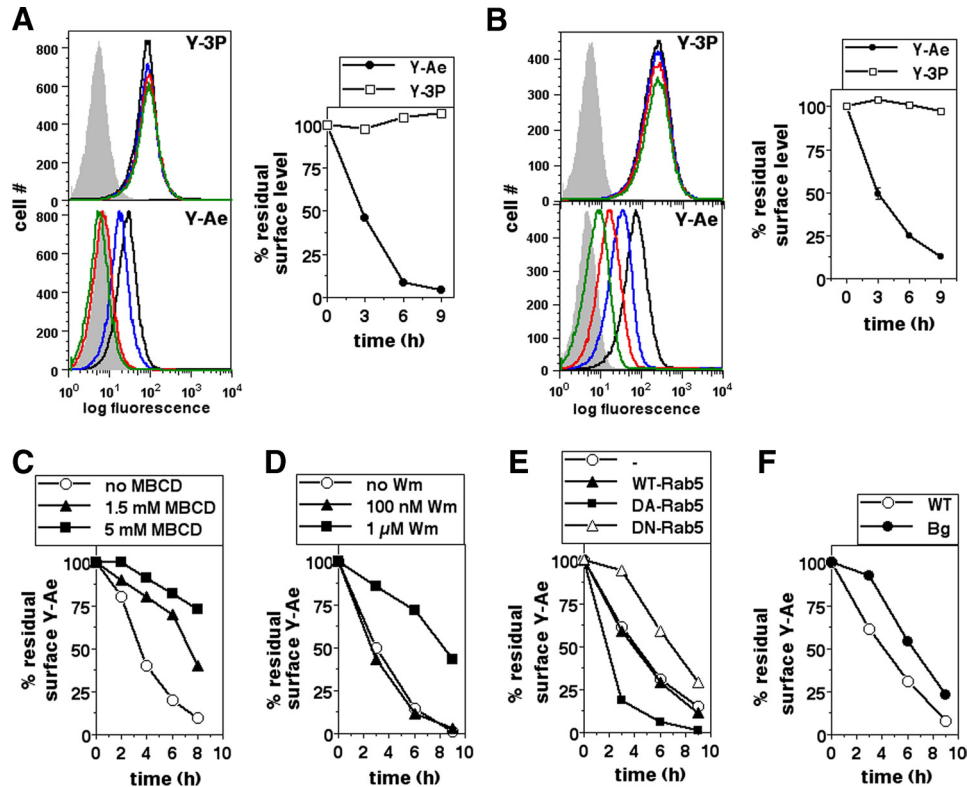
For this, BMC-2 cells were pulsed with Eap for 1 h at 37°C and labeled with biotinylated Y-Ae at 4°C as above, followed by incubation for varying times in the presence or absence of MBCD or Wm before the detection of levels remaining at the cell surface. The pMHCII complexes were lost more slowly from the surface if cholesterol was chelated (Fig. 6C). Also, although a low Wm concentration did not affect the rate of removal of pMHCII complexes, a higher concentration, which has been reported to inhibit other PIKs in addition to PI3K (33), also retarded the loss of surface pMHCII (Fig. 6D).

To examine the role of Rab5, BMC-2 cells were transfected with constructs driving the expression of WT Rab5-eGFP, DN Rab5-eGFP, or CA Rab5-eGFP. Cells were pulsed 12 h posttransfection with Eap and labeled with Y-Ae as above and incubated for varying times before the detection of residual surface levels. The pMHCII complexes were lost more slowly from the surface of DN Rab5-expressing cells, while they were lost more rapidly in CA Rab5-expressing cells (Fig. 6E).

We also examined the rate of loss of surface pMHCII complexes from WT and Bg cells. As described above, BMDMs grown from either WT or Bg mice were used. Cells were pulsed with Eap and labeled with Y-Ae as above and the loss of surface label was tracked. Bg BMDMs showed a slower loss of surface pMHCII complexes compared with WT cells (Fig. 6F).

In similar assays, we also examined the effect of blocking molecular activities crucial for Nef-mediated removal of other cell

FIGURE 6. Peptide-MHCII complexes are removed from the cell surface by a mechanism at least partially dependent on cholesterol, PIK, Rab5, and Lyst. *A*, BMC-2 cells were pulsed with Eap for 60 min and cultured for 0 h (black line), 3 h (blue line), 6 h (red line), or 9 h (green line) before staining with either the pMHCII-specific mAb Y-Ae or the H-2Ab -specific mAb Y-3P for flow cytometry. Gray curves indicate isotype controls. Mean fluorescence intensities were calculated for HAp-gated cells and the data normalized to the starting intensities as a percentage of the residue of surface label. *B*, BMC-2 cells were pulsed with Eap for 60 min and stained with either Y-Ae or Y-3P and cultured for 0 h (black line), 3 h (blue line), 6 h (red line), or 9 h (green line) before flow cytometric detection of residual cell surface label. Gray curves indicate isotype controls. Mean fluorescence intensities were calculated and the data normalized to the starting intensities as a percentage of the residue of surface label. *C* and *D*, BMC-2 cells were pulsed with Eap for 60 min and stained with either Y-Ae or Y-3P and cultured for various times in the presence or absence of various concentrations of MBCD (*C*) or Wm (*D*) as indicated before detection of the residual cell surface label. Mean fluorescence intensities were calculated and the data normalized to the starting intensities as a percentage of the residue of surface label. *E*, BMC-2 cells transfected to express either eGFP alone or with WT Rab5, CA Rab5, or DN Rab5 as indicated were pulsed with Eap for 60 min and stained with either Y-Ae or Y-3P and cultured for various times as shown before detection of the residual cell surface label. Mean fluorescence intensities were calculated and the data normalized to the starting intensities as a percentage of the residue of the surface label. *F*, BMDMs derived from WT C57BL/6 or *bg/bg* (Bg) mice were pulsed with Eap for 60 min and stained with either Y-Ae or Y-3P and cultured for various times as indicated before detection of residual cell surface label. Mean fluorescence intensities were calculated and the data normalized to the starting intensities as a percentage of the residue of surface label.

surface molecules on the rate of pMHCII removal. Blocking the activities of WASP, Dyn, or Eps15 had no effect on the rate of loss of pMHCII complexes from the surface of BMC-2 cells (data not shown).

Together, these data indicate that short-lived pMHCII complexes on mouse monocytic cells, even in the absence of Nef, are removed from the cell surface by an endocytotic mechanism dependent on cholesterol, PIK, Rab5, and Lyst. This concordance between the trafficking pathways of total cell surface MHCII in Nef-expressing cells and those of specific pMHCII complexes in non-Nef-expressing cells suggests that Nef may be subverting constitutive pathways of MHCII endocytosis for the removal of cell surface MHCII molecules.

Discussion

In epithelial cells expressing the CIITA, Nef has been reported to affect MHCII-mediated Ag presentation by altering the intracellular trafficking of MHCII molecules to reduce the levels of mature MHCII and increase immature MHCII on the cell surface (9). Because Ii-associated immature MHCII is functionally incompetent, an immune evasion function has been suggested (9). The delivery

of immature MHCII to the lysosomes is also impaired, resulting in reduced Ii degradation (17). However, in the presence of Nef, MHCII is found at high levels in intracellular lysosomal compartments. Our results now extend these findings to professional APCs of the myeloid lineage and identify some molecular intermediates used by Nef to induce surface MHCII-down-regulation. We find that this pathway is similar to that used in constitutive endocytosis of peptide-MHCII complexes, indicating that Nef subverts a preexisting MHCII endocytic program.

Human as well as mouse myeloid cells are sensitive to these effects of Nef, and these observations are consistent between cell lines and primary monocytes of both human and mouse origin. The phenomenon is likely to be of some pathophysiological significance, because Nef-dependent loss of cell surface MHCII is seen on HIV-1 infection, although there are significant differences between the laboratory strain of HIV-1 and clinical isolates, raising the possibility of interesting variations in this property in the latter group. The loss of cell surface MHCII in monocytic cells expressing Nef is not accompanied by any loss of total cellular levels of MHCII, indicating that Nef mediates a cellular redistribution of MHCII. This characteristic is also seen with regard to MHCI,

including our observation of a clinical isolate that is inefficient in the down-modulation of MHCI and MHCII, but not in that of CD80 and CD86.

The removal of cell surface MHCII could be the result of reduced delivery to the cell surface and/or enhanced removal by endocytosis. Unlike the case for MHCI, CD80, and CD86 (Ref. 7 and data not shown), MHCII delivery to the cell surface is retarded in Nef-expressing cells. However, Nef induces endocytic removal of all four of these target molecules. The eventual intracellular destinations of these molecules in Nef-expressing cells, are however, quite distinct. Although MHCI, CD80, and CD86 are removed to the Golgi region, MHCII relocates to the lysosomal compartment.

Similarly, the differences between the vesicular trafficking pathways followed by these target molecules in Nef-expressing cells are different and noteworthy. We observed recently that CD80 and CD86 are internalized into vesicles that do not show any markers of endosomal compartments and that they recruit Rab11 after a lag of some hours, using Rab11 activity for cargo delivery to the Golgi, although Rab11 activity is not required for the Golgi localization of MHCI (40). In contrast, both MHCI (41) and MHCII enter early endosomal compartments marked by Rab5 and either fluid cargo and/or Tf. However, their pathways then diverge. MHCI molecules go on to the sorting compartment marked by Arf6 and then to the Golgi apparatus (41), whereas MHCII molecules move to the late endosomes marked by Rab7 and then to a LAMP-1-bearing lysosomal compartment using Rab7 activity.

Similarly, we find that the molecular intermediates involved in the Nef-mediated endocytosis of these four target molecules show major differences. CD80 and CD86 follow a unique endocytosis pathway defined by its dependence on protein kinase C, c-Src, TIAM, Rac, and actin and by being independent of cholesterol, clathrin, Dyn, and PIK activity (24). In fact, we have not to date found any molecular intermediates shared by CD80/CD86 on the one hand and MHCI/MHCII on the other. However, MHCI and MHCII also show striking differences in the signaling intermediates used for their Nef-mediated endocytosis. Although both are cholesterol- and PIK-dependent and Dyn-independent, MHCI appears to use some form of the clathrin-adaptor complex whereas MHCII does not. Although both enter Rab5-containing vesicles, MHCI endocytosis does not depend on Rab5 or Lyst activity, whereas MHCII endocytosis does.

It is thus possible to argue for a model in which recycling MHCI enters sorting endosomes for a decision on whether they will be recycled back to the cell surface or not, which is where Nef may intervene and reroute them to the Golgi apparatus (41). However, MHCII molecules may recycle through an early endosomal compartment dependent on the homologous fusion of early endosomes controlled by Rab5 so that the lack of Rab5 activity may lead to default delivery to late endosomes and then by normal endolysosomal Rab7-dependent maturation mechanisms to the lysosomes. Because Bg cells show defective trafficking to the late endosomal compartments and increased ability of these lysosomes to fuse with the plasma membrane (42, 43), the loss of Nef-mediated MHCII down-regulation in Bg cells can perhaps be explained either by enhanced recycling back to the cell surface from early endosomes and/or by fusion of Bg lysosomes with the plasma membrane.

Such organized and branching cascades of signaled traffic suggests that Nef may be using pre-existing pathways normally used for the control of trafficking and turnover for these molecules. It is also of interest in this connection to note that, although Nef does bind to the cytosolic tails of CD80 and CD86 directly, evidence regarding its recruitment to the cytoplasmic portions of either MHCI or MHCII is sparse (9, 44), suggesting a possible alteration

of normal turnover pathways rather than a directly induced endocytosis. We examined this possibility by testing whether peptide-MHCII complexes on the cell were normally internalized and, if so, whether the signaling intermediates needed for Nef-dependent removal of cell surface MHCII were also involved in the normal removal of pMHCII complexes. Our data indicate that pMHCII complexes are short lived on the cell surface and that their loss is indeed significantly dependent on cholesterol, PIK, Rab5, and Lyst activity.

There is thus a considerable degree of overlap between the molecular intermediates that are involved in the removal of Y-Ae-reactive pMHCII complexes from the APC surface and those involved in the Nef-induced internalization of MHCII molecules. Both endocytic programs are sensitive to cholesterol depletion, require PIK activity, are dependent on Lyst as well as Rab5 function, and intracellular trafficking of the internalized complexes is Rab7 dependent. Thus, Nef appears to subvert a constitutive endocytic program that removes pMHCII complexes from the cell surface to mediate the removal of all MHCII molecules from the cell surface. How does Nef mediate the accelerated removal of MHCII molecules by such a constitutive pathway? In this context, an interesting difference between Nef-mediated MHCII removal and constitutive removal of pMHCII complexes is notable. The constitutive program appears to remove specific pMHCII complexes rapidly from the cell surface over time without affecting the equilibrium MHCII levels, whereas Nef extends this short-lived property to all cell surface MHCII molecules. Nef clearly retards the exocytosis of newly formed MHCII molecules, including their delivery to the endolysosomal compartments (17), and we have observed in preliminary experiments that that inhibition of protein synthesis in normal APCs leads to a rapid loss of pre-existing cell surface MHCII molecules (data not shown). It is thus possible to visualize an intriguingly novel model in which the recycling of MHCII from endosomal compartments is dependent on the availability of new peptide as well as MHCII in those compartments, and their lack leads to a sorting decision in favor of lysosomal delivery. Further studies will be needed to establish the validity and mechanisms of such a process.

Acknowledgments

Disclosures

The authors declare that they have no competing financial interests.

References

1. Kestler, H. W., III, D. J. Ringler, K. Mori, D. L. Panicali, P. K. Sehgal, M. D. Daniel, and R. C. Desrosiers. 1991. Importance of the *nef* gene for maintenance of high virus loads and for development of AIDS. *Cell* 65: 651–662.
2. Hanna, Z., D. G. Kay, N. Rebai, A. Guimond, S. Jothy, and P. Jolicoeur. 1998. Nef harbors a major determinant of pathogenicity for an AIDS-like disease induced by HIV-1 in transgenic mice. *Cell* 95: 163–175.
3. Miller, M. D., M. T. Warmerdam, I. Gaston, W. C. Greene, and M. B. Feinberg. 1994. The human immunodeficiency virus-1 *nef* gene product: a positive factor for viral infection and replication in primary lymphocytes and macrophages. *J. Exp. Med.* 179: 101–113.
4. Das, S. R., and S. Jameel. 2005. Biology of the HIV Nef protein. *Indian J. Med. Res.* 121: 315–332.
5. Arold, S. T., and A. S. Baur. 2001. Dynamic Nef and Nef dynamics: how structure could explain the complex activities of this small HIV protein. *Trends Biochem. Sci.* 26: 356–363.

6. Geyer, M., O. T. Fackler, and B. M. Peterlin. 2001. Structure-function relationships in HIV-1 Nef. *EMBO Rep.* 2: 580–585.

7. Chaudhry, A., S. R. Das, A. Hussain, S. Mayor, A. George, V. Bal, S. Jameel, and S. Rath. 2005. The Nef protein of HIV-1 induces loss of cell surface costimulatory molecules CD80 and CD86 in APCs. *J. Immunol.* 175: 4566–4574.

8. Schwartz, O., V. Marechal, S. Le Gall, F. Lemonnier, and J. M. Heard. 1996. Endocytosis of major histocompatibility complex class I molecules is induced by the HIV-1 Nef protein. *Nat. Med.* 2: 338–342.

9. Stumptner-Cuvelette, P., S. Morchoisne, M. Dugast, S. Le Gall, G. Raposo, O. Schwartz, and P. Benaroch. 2001. HIV-1 Nef impairs MHC class II antigen presentation and surface expression. *Proc. Natl. Acad. Sci. USA* 98: 12144–12149.

10. Oxenius, A., M. F. Bachmann, P. G. Ashton-Rickardt, S. Tonegawa, R. M. Zinkernagel, and H. Hengartner. 1995. Presentation of endogenous viral proteins in association with major histocompatibility complex class II: on the role of intracellular compartmentalization, invariant chain and the TAP transporter system. *Eur. J. Immunol.* 25: 3402–3411.

11. Hegde, N. R., M. S. Chevalier, and D. C. Johnson. 2003. Viral inhibition of MHC class II antigen presentation. *Trends Immunol.* 24: 278–285.

12. Bakke, O., and B. Dobberstein. 1990. MHC class II-associated invariant chain contains a sorting signal for endosomal compartments. *Cell* 63: 707–716.

13. Neefjes, J. 1999. CIIV, MIIC and other compartments for MHC class II loading. *Eur. J. Immunol.* 29: 1421–1425.

14. Geuze, H. J. 1998. The role of endosomes and lysosomes in MHC class II functioning. *Immunol. Today* 19: 282–287.

15. Reid, P. A., and C. Watts. 1992. Constitutive endocytosis and recycling of major histocompatibility complex class II glycoproteins in human B-lymphoblastoid cells. *Immunology* 77: 539–542.

16. Harding, C. V., and E. R. Unanue. 1989. Antigen processing and intracellular Ia. Possible roles of endocytosis and protein synthesis in Ia function. *J. Immunol.* 142: 12–19.

17. Stumptner-Cuvelette, P., M. Jouve, J. Helft, M. Dugast, A. S. Glouzman, K. Jooss, G. Raposo, and P. Benaroch. 2003. Human immunodeficiency virus-1 Nef expression induces intracellular accumulation of multivesicular bodies and major histocompatibility complex class II complexes: potential role of phosphatidylinositol 3-kinase. *Mol. Biol. Cell* 14: 4857–4870.

18. Schindler, M., S. Wurfl, P. Benaroch, T. C. Greenough, R. Daniels, P. Easterbrook, M. Brenner, J. Munch, and F. Kirchhoff. 2003. Down-modulation of mature major histocompatibility complex class II and up-regulation of invariant chain cell surface expression are well-conserved functions of human and simian immunodeficiency virus *nef* alleles. *J. Virol.* 77: 10548–10556.

19. Conner, S. D., and S. L. Schmid. 2003. Regulated portals of entry into the cell. *Nature* 422: 37–44.

20. Johannes, L., and C. Lamaze. 2002. Clathrin-dependent or not: is it still the question? *Traffic* 3: 443–451.

21. Sabharanjak, S., P. Sharma, R. G. Parton, and S. Mayor. 2002. GPI-anchored proteins are delivered to recycling endosomes via a distinct *cdc42*-regulated, clathrin-independent pinocytic pathway. *Dev. Cell* 2: 411–423.

22. Dani, A., A. Chaudhry, P. Mukherjee, D. Rajagopal, S. Bhatia, A. George, V. Bal, S. Rath, and S. Mayor. 2004. The pathway for MHCII-mediated presentation of endogenous proteins involves peptide transport to the endo-lysosomal compartment. *J. Cell Sci.* 117: 4219–4230.

23. Chatterjee, S., E. R. Smith, K. Hanada, V. L. Stevens, and S. Mayor. 2001. GPI anchoring leads to sphingolipid-dependent retention of endocytosed proteins in the recycling endosomal compartment. *EMBO J.* 20: 1583–1592.

24. Chaudhry, A., S. R. Das, S. Jameel, A. George, V. Bal, S. Mayor, and S. Rath. 2007. A two-pronged mechanism for HIV-1 Nef-mediated endocytosis of immune costimulatory molecules CD80 and CD86. *Cell Host Microbe* 1: 37–49.

25. Dunn, K. W., T. E. McGraw, and F. R. Maxfield. 1989. Iterative fractionation of recycling receptors from lysosomally destined ligands in an early sorting endosome. *J. Cell Biol.* 109: 3303–3314.

26. Kirkham, M., A. Fujita, R. Chadda, S. J. Nixon, T. V. Kurzchalia, D. K. Sharma, R. E. Pagano, J. F. Hancock, S. Mayor, and R. G. Parton. 2005. Ultrastructural identification of uncoated caveolin-independent early endocytic vehicles. *J. Cell Biol.* 168: 465–476.

27. Mayor, S., J. F. Presley, and F. R. Maxfield. 1993. Sorting of membrane components from endosomes and subsequent recycling to the cell surface occurs by a bulk flow process. *J. Cell Biol.* 121: 1257–1269.

28. Ghosh, R. N., D. L. Gelman, and F. R. Maxfield. 1994. Quantification of low density lipoprotein and transferrin endocytic sorting HEp2 cells using confocal microscopy. *J. Cell Sci.* 107: 2177–2189.

29. Hussain, A., C. Wesley, M. Khalid, A. Chaudhry, and S. Jameel. 2008. Human immunodeficiency virus type 1 Vpu protein interacts with CD74 and modulates major histocompatibility complex class II presentation. *J. Virol.* 82: 893–902.

30. Stenmark, H., R. G. Parton, O. Steele-Mortimer, A. Lutcke, J. Gruenberg, and M. Zerial. 1994. Inhibition of rab5 GTPase activity stimulates membrane fusion in endocytosis. *EMBO J.* 13: 1287–1296.

31. Faigle, W., G. Raposo, D. Tenza, V. Pinet, A. B. Vogt, H. Kropshofer, A. Fischer, G. de Saint-Basile, and S. Amigorena. 1998. Deficient peptide loading and MHC class II endosomal sorting in a human genetic immunodeficiency disease: the Chediak-Higashi syndrome. *J. Cell Biol.* 141: 1121–1134.

32. Larsen, J. E., R. H. Massol, T. J. Nieland, and T. Kirchhausen. 2004. HIV Nef-mediated major histocompatibility complex class I down-modulation is independent of Arf6 activity. *Mol. Biol. Cell* 15: 323–331.

33. Wymann, M. P., G. Bulgarelli-Leva, M. J. Zvelebil, L. Pirola, B. Vanhaesebroeck, M. D. Waterfield, and G. Panayotou. 1996. Wortmannin inactivates phosphoinositide 3-kinase by covalent modification of Lys-802, a residue involved in the phosphate transfer reaction. *Mol. Cell Biol.* 16: 1722–1733.

34. Le Gall, S., F. Buseyne, A. Trocha, B. D. Walker, J. M. Heard, and O. Schwartz. 2000. Distinct trafficking pathways mediate Nef-induced and clathrin-dependent major histocompatibility complex class I down-regulation. *J. Virol.* 74: 9256–9266.

35. Damke, H., T. Baba, D. E. Warnock, and S. L. Schmid. 1994. Induction of mutant dynamin specifically blocks endocytic coated vesicle formation. *J. Cell Biol.* 127: 915–934.

36. Gomez, T. S., M. J. Hamann, S. McCarney, D. N. Savoy, C. M. Lubking, M. P. Heldebrant, C. M. Labno, D. J. McKean, M. A. McNiven, J. K. Burkhardt, and D. D. Billadeau. 2005. Dynamin 2 regulates T cell activation by controlling actin polymerization at the immunological synapse. *Nat. Immunol.* 6: 261–270.

37. Benmerah, A., V. Poupon, N. Cerf-Bensussan, and A. Dautry-Varsat. 2000. Mapping of Eps15 domains involved in its targeting to clathrin-coated pits. *J. Biol. Chem.* 275: 3288–3295.

38. Simpson, F., N. K. Hussain, B. Qualmann, R. B. Kelly, B. K. Kay, P. S. McPherson, and S. L. Schmid. 1999. SH3-domain-containing proteins function at distinct steps in clathrin-coated vesicle formation. *Nat. Cell Biol.* 1: 119–124.

39. Rudensky, A., S. Rath, P. Preston-Hurlburt, D. B. Murphy, and C. A. Janeway, Jr. 1991. On the complexity of self. *Nature* 353: 660–662.

40. Chaudhry, A., S. R. Das, S. Jameel, A. George, V. Bal, S. Mayor, and S. Rath. 2008. HIV-1 Nef induces a Rab11-dependent routing of endocytosed immune costimulatory proteins CD80 and CD86 to the Golgi. *Traffic* 9: 1925–1935.

41. Blagoveshchenskaya, A. D., L. Thomas, S. F. Feliciangeli, C. H. Hung, and G. Thomas. 2002. HIV-1 Nef downregulates MHC-I by a PACS-1- and PI3K-regulated ARF6 endocytic pathway. *Cell* 111: 853–866.

42. Huynh, C., D. Roth, D. M. Ward, J. Kaplan, and N. W. Andrews. 2004. Defective lysosomal exocytosis and plasma membrane repair in Chediak-Higashi/beige cells. *Proc. Natl. Acad. Sci. USA* 101: 16795–16800.

43. Brandt, E. J., R. W. Elliott, and R. T. Swank. 1975. Defective lysosomal enzyme secretion in kidneys of Chediak-Higashi (beige) mice. *J. Cell Biol.* 67: 774–788.

44. Williams, M., J. F. Roeth, M. R. Kasper, R. I. Fleis, C. G. Przybycin, and K. L. Collins. 2002. Direct binding of human immunodeficiency virus type 1 Nef to the major histocompatibility complex class I (MHC-I) cytoplasmic tail disrupts MHC-I trafficking. *J. Virol.* 76: 12173–12184.